Journal of Materials Chemistry C

Bis(Tercarbazole) Pyrene and Tetrahydropyrene Derivatives: Photophysical and Electrochemical Properties, Theoretical Modeling, and OLEDs

Journal:	*Journal of Materials Chemistry C*
Manuscript ID	TC-ART-12-2018-006266.R1
Article Type:	Paper
Date Submitted by the Author:	06-Mar-2019
Complete List of Authors:	Kaafarani, Bilal; American University of Beirut, Department of Chemistry El-Assaad, Tarek; American University of Beirut, Department of Chemistry Smith, William ; University of Kentucky Ryno, Sean ; University of Kentucky Hermerschmidt, Felix; Humboldt-Universität zu Berlin, Institut für Physik, Institut für Chemie Lyons, Jeffrey; Humboldt-Universität zu Berlin, Institut für Physik, Institut für Chemie Patra, Digambara; American University of Beirut, Chemistry Wex, Brigitte; Lebanese American University, Natural Sciences List-Kratochvil, Emil; Institut für Physik, Institut für Chemie, and IRIS Adlershof, Humboldt-Universität zu Berlin, Risko, Chad; University of Kentucky, Chemistry Barlow, Stephen; Georgia Institute of Technology, School of Chemistry and Biochemistry Marder, Seth; Georgia Institute of Technology, School of Chemistry and Biochemistry

Bis(Tercarbazole) Pyrene and Tetrahydropyrene Derivatives: Photophysical and Electrochemical Properties, Theoretical Modeling, and OLEDs

Bilal R. Kaafarani,[1,*] Tarek H. El-Assaad,[1] William A. Smith,[2] Sean M. Ryno,[2] Felix Hermerschmidt,[3] Jeffrey Lyons,[3] Digambara Patra,[1] Brigitte Wex,[4] Emil J. W. List-Kratochvil,[3] Chad Risko,[2] Stephen Barlow,[5] Seth R. Marder[5]

[1] American University of Beirut, Department of Chemistry, Beirut, Lebanon

[2] Department of Chemistry and Center for Applied Energy Research (CAER), University of Kentucky, Lexington, KY 40506-0055, USA

[3] Humboldt-Universität zu Berlin, Institut für Physik, Institut für Chemie, IRIS Adlershof, Brook-Taylor-Str. 6, 12489 Berlin, Germany

[4] Department of Natural Sciences, Lebanese American University, Byblos, Lebanon

[5] Center for Organic Photonics and Electronics, School of Chemistry and Biochemistry, Georgia Institute of Technology, Atlanta, GA 30332-0400, USA

Abstract

2,7-Bis(3,3",6,6"-tetra(*tert*-butyl)-9'*H*-9,3':6',9"-tercarbazol-9-yl)-4,5,9,10-tetrahydropyrene (**3**) and 2,7-bis(3,3",6,6"-tetra(*tert*-butyl)-9'*H*-9,3':6',9"-tercarbazol-9-yl)pyrene (**4**), along with a model compound, 3,3",6,6"-tetra(*tert*-butyl)-9'-(4-(*tert*-butyl)phenyl)-9'H-9,3':6',9"-tercarbazole (**6**), have been synthesized using microwave-assisted palladium-catalyzed couplings and compared to analogous 3,6-di(*tert*-butyl)carbazol-9-yl species (**1**, **2**, and **5**). Time-dependent density functional theory (TDDFT) calculations reveal absorptions with quadrupolar (ter)carbazole-to-bridge CT character for **1**-**4**. Compound **4** is unusual in showing dual fluorescence in a number of solvents, the longer wavelength of which is markedly more solvatochromic compared to the bands of the other compounds. Following the observed three oxidations on the TCz model compound **6**, compounds **3** and **4** can be electrochemically reversibly oxidized to hexacations with four oxidation and three oxidation steps of a 2:2:1:1 and 2:2:2 ratio, respectively. Tercarbazole derivatives **3** and **4** have been used as the emissive layers of simple solution-processed few-layer organic light-emitting diodes.

Keywords: Carbazole, tercarbazole, photophysical studies, OLED

* To whom correspondence should be addressed. Email: bilal.kaafarani@aub.edu.lb

Introduction

Carbazole is a widely used building block in the field of organic electronics and photonics, and has been incorporated into molecules and polymers for one- and two-photon fluorescent sensing,[1] two-photon photoinitiation of polymerization,[2] optical power limiting,[3, 4] photorefractive composites for holographic imaging,[5] and solar energy harvesting.[6-8] These applications generally rely on the carbazole moiety acting as a moderate electron donor, either in a π-donor sense or an electron-transfer sense,[9] and/or its hole-transport abilities. These same properties have also led to extensive use of carbazole materials in organic light-emitting diodes (OLEDs), both as hole-transport materials and emitters.[10]

Carbazoles have been extensively used as building blocks for materials for emissive layers of both first-generation fluorescence-based devices[11, 12] and, primarily as components of host materials in second-generation phosphorescence-based devices (PHOLEDs);[13, 14] more recently they have been used as building blocks for both emitters and host materials for OLEDs based on thermally-activated delayed fluorescence (TADF).[15-21] Carbazole has an appropriate ionization potential (IE) to inject holes to and from relevant layers in OLEDs,[22] and many examples exhibit good film-forming abilities[23] and adequate good hole mobilities.[6, 24-26] In addition, the high triplet energy[27] of approximately 3.0 eV[28] of the carbazole moiety is particularly attractive for use in host materials for phosphorescent and TADF emitters,[23, 29] and, when linked to suitable acceptors, for the development of molecules with low singlet-triplet energy separations that exhibit TADF.[30, 31] Derivatives of 9'*H*-9,3':6',9"-tercarbazole[32-40] have also been shown to have useful electronic and hole-transporting properties; these retain the high triplet energy and hole-transport properties of simple carbazoles, but generally exhibit higher glass-transition temperatures, as well as acting as somewhat stronger donors.

We have previously reported blue-emitting compounds bis(carbazol-9-yl) or bis(3,6-di(*tert*-butyl)carbazol-9-yl) derivatives of benzene, biphenyl, pyrene (Py) and 4,5,9,10-tetrahydropyrene (THPy), including **1** and **2** (Figure 1), which exhibit some donor-acceptor-donor (D-A-D) characteristics.[41] Here, we report the synthesis of new D-A-D compounds where D = 3,3",6,6"-tetra(*tert*-butyl)-9'*H*-9,3':6',9"-tercarbazol-9-yl, TCz', and A = Py, THPy (**3** and **4**, respectively; Figure 1). The photophysical properties of these compounds are compared to those of the analogous Cz' species (**1** and **2**), and to Cz' and TCz' model compounds (**5** and **6**), density functional theory (DFT) and time-dependent DFT (TDDFT) calculations are used to gain insight into the key frontier molecular orbitals, ionization

energies, and electronic transitions, and the molecules are used as the emissive layer of OLEDs.

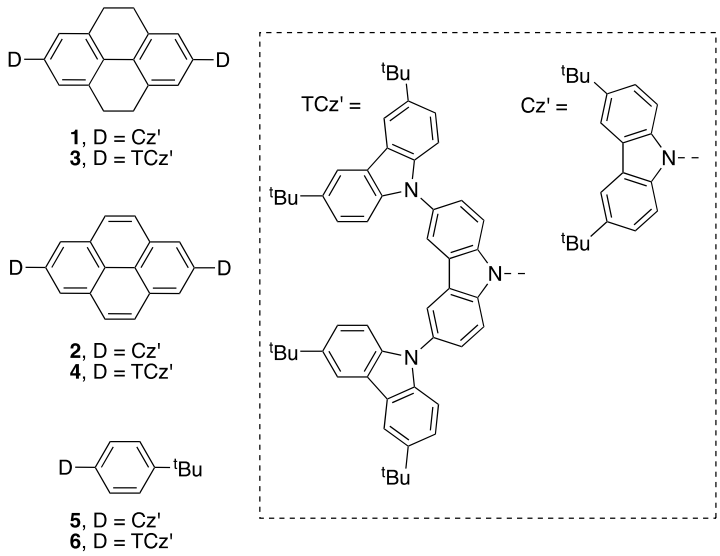

Figure 1. Structures of the compounds discussed in this work.

Results and discussion

Synthesis

Our target compounds are shown in Figure 1. The *tert*-butyl substituents in the 3,6 positions of the terminal carbazolyl groups of the tercarbazole moieties of **3** and **4** are anticipated to afford cleaner electrochemical behavior and potentially better stability under device operation as a hole-transport material since these substituents block the sites through which carbazole radical cations can dimerize or polymerize.[42, 43] Indeed, we have previously found that **1** and **2** exhibit reversible electrochemistry, whereas their non-*tert*-butyl substituted analogues do not.[41] In addition, an increase in thermal stability[44] is expected. Moreover, the nitrogen position of the central carbazole units of the model compounds is protected with a 4-*tert*-butylphenyl group. We note that a molecule closely related to model compound **6** entitled **BTCC-36**, with a 9'-phenyl rather than a 9'-(4-*tert*-butylphenyl), has previously been utilized as host for PHOLEDs.[29] We have previously described the synthesis of compounds **1**, **2**, and **5** through the Buchwald-Hartwig coupling of the appropriate (di)bromoarenes (**7**-**9**, respectively) with 3,6-di-*tert*-butylcarbazole (**10**) using microwave irradiation.[41, 45] The new compounds **3**, **4**, and **6** were synthesized in the same way, as shown in Scheme 1, using 3,3",6,6"-tetra-*tert*-butyl-9'*H*-9,3':6',9"-tercarbazole, TCz'H (**11**)[46] in place of **10**.

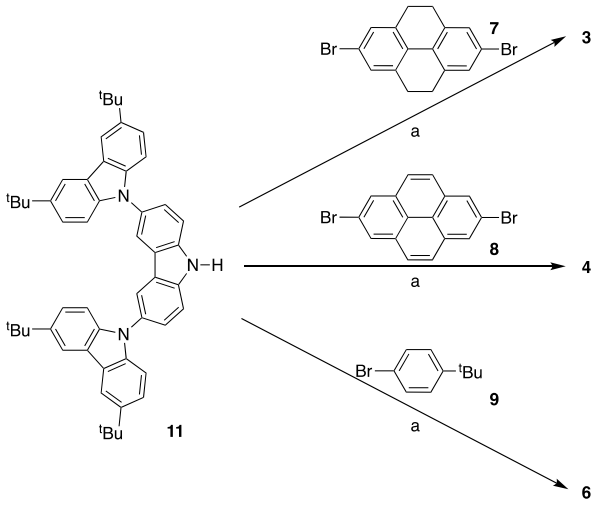

Scheme 1. Synthesis of tercarbazole derivatives **3**, **4**, and **6** using conditions previously used to synthesize **1**, **2**, and **5**.[41, 45] (a) Tris(dibenzylideneacetone)dipalladium(0), tri-*tert*-butylphosphine, sodium *tert*-butoxide, dry toluene, inert anhydrous atmosphere, microwave oven (power: 180 W; maximum temp: 125 °C; run time: 2 min; hold time: 60 min; pressure: 120 psi).

Geometric and Electronic Structure

Before discussing the photophysical and electrochemical characteristics of **1**-**6**, we describe the molecular geometric and electronic characteristics via density functional theory (DFT) calculations at the OT-ωB97X-D/6-31g(d,p) level of theory. We note that the geometric, electronic, redox, and optical (via time-dependent DFT [TDDFT]) properties of **1**, **2**, and **5** have previously been evaluated at the B3LYP/6-31G(d,p) level of theory.[41, 45] The results from the two levels of DFT and TDDFT calculations are comparable; hence we will focus solely on data derived from the OT-ωB97X-D/6-31g(d,p) level in this work.

The THPy bridge is, as expected, twisted for the neutral ground states (S_0) of **1** and **3**, with the biphenyl-like structure possessing a twist of 17°, whereas the Py bridges of ground-state **2** and **4** are planar. For all compounds **1**-**6**, the bridging N(carbazole)–C(aryl bridge) bonds are approximately 1.42 Å, with the carbazole moieties presenting a significant twist (ranging

from 56–65°) with respect to the aryl bridge. The twist angles among the different carbazoles of the TCz' groups of **3**, **4**, and **6** range from 62–65°.

Though the geometries are rather similar regardless of whether the molecules have THPy or Py bridges, the molecular orbitals (MO) present some notable differences. For **1** and **2**, which contain single carbazole moieties attached to the THPy and Py bridges, respectively, the highest-occupied MO (HOMO) show a high degree of delocalization across both Cbz' end groups and the bridging moiety, though in **2** (E_{HOMO} = –6.79 eV) the contribution from the bridging Py is smaller than that from the THPy in **1** (–6.54 eV).[41] To understand the frontier occupied MO for **3** and **4**, it is instructive to examine those of **6**, where the HOMO (–6.71 eV) and HOMO–1 (–6.82 eV) are both distributed across the TCz' unit (pictorial representations of select frontier MO of **3**, **4**, and **6** can be found in the Electronic Supplementary Information). For **3** and **4**, the HOMO (–6.50 eV and –6.61 eV, respectively) and HOMO–1 (–6.51 eV and –6.62 eV, respectively) are almost iso-energetic and represent the linear combinations of the tercarbazole-based HOMO observed in **6**. There are little-to-no contributions of the ThPy or Py bridges to the HOMO, and, in fact, the HOMOs are pushed mainly out onto the four perimeter carbazole units, with only modest contributions from the carbazole nitrogen atoms attached to the THPy or Py bridges. In addition, the HOMO–2 (–6.62 eV and –6.72 eV, respectively) and HOMO–3 (–6.62 eV and –6.72 eV, respectively) are essentially linear combinations of the HOMO–1 of two **6**-like units, and are nearly degenerate. The lowest-unoccupied molecular orbitals (LUMO), on the other hand, for **1**-**4** are each bridge localized, imparting D-A-D character to the molecules.

Photophysical properties

The UV-visible absorption spectra of **1**-**6** were recorded in chloroform and THF and are depicted in Figure 2. The bands centered around 290 nm are attributed to localized transitions associated with the carbazole core, while the absorption bands of lower intensity occurring

above 300 nm are attributed to π→π* transitions of the chromophore, as previously reported for **1** and **2**.[41] As shown in Tables 1 and 2, the longest wavelength absorption bands of the TCz' compounds are seen at the same, or almost same, wavelength as their Cz' analogues.[41]

TDDFT at the OT-ωB97X-D/6-31g(d,p) level of theory reveal the variations in the π→π* transitions for **1**-**4**. For **1** and **2**, the $S_0 \rightarrow S_1$ transitions are at 3.84 eV (323 nm) and 3.49 eV (356 nm); these results are in good qualitative agreement with experiment and previous TDDFT B3LYP/6-31G(d,p) calculations.[41] These transitions are well described as HOMO → LUMO one-electron excitations, where the natural transition orbitals (NTO) reveal some D-to-A quadrupolar charge-transfer character, the respective holes being delocalized across the entire molecule (including the carbazole unit) with the electron mainly localized on the THPy (**1**) or Py (**2**) bridge. The slightly red-shifted transition for **2** is attributable to the more extended π-conjugated structure of the Py bridge, which results in a lower lying LUMO. For **3** and **4** with the tercarbazole moieties, a similar picture arises, though in both instances it is the $S_0 \rightarrow S_3$ transitions that are the lowest-lying to exhibit appreciable oscillator strength: 3.88 eV (319 nm) for **3** and 3.80 eV (327 nm) for **4**. The NTO (see ESI for pictorial representations) reveal that the holes in both instances are generally delocalized, and more so in 3, although they only extend onto the carbazole unit that is directly bonded with the bridging aryl unit (i.e., resembling the hole wavefunctions for **1** and **2** as previously reported), and the electron is bridge-localized, meaning the transitions have some carbazole-to-bridge quadrupolar charge-transfer character.

The fluorescence spectra of **1**-**6** were recorded in chloroform and THF (Figures 2B and 2D). The maximum for the fluorescence of the model monomeric TCz' derivative **6** is bathochromically shifted (by 0.23 and 0.17 eV in chloroform and THF, respectively) with respect to that of its Cz' analogue, **5**. Similarly, the emission maximum of the THPy-bridged bis-TCz' derivative, **3**, is bathochromically-shifted by 0.16-0.17 eV relative to that of its bis-

Cz' analogue, **1**. Moreover, the emissions of the THPy-bridged examples are seen at similar energies as those of the mono-Cz' or TCz' model compounds. On the other hand, the emissions of Py-bridged **2** and **4** are significantly bathochromically-shifted relative to their THP analogues, with that of **4** being particular dramatically bathochromically-shifted and Stokes shifted (Figure 3). On closer inspection, it is clear that **4** exhibits two emission bands, the principal, highly Stokes-shifted peak (lower in energy), and a weaker shoulder or peak (higher in energy) at similar wavelengths to the emissions of the THP-bridged and *tert*-butylphenyl derivatives. It also appears that **2** exhibits a distinct short-wavelength feature as a shoulder on the main emission. DFT calculations suggest the lowest energy absorption has some Cz/TCz-to-Py CT character. The higher-energy of the two emission bands has a similar Stokes shifts to the THP and model compounds. Accordingly, the higher energy emission is expected to have a similar origin to the lowest energy absorption; the lower energy emission might, for example, originate from a TICT-like relaxation of the higher energy state.[47]

The photoluminescence of these compounds was further investigated for a wider range of solvents exhibiting a large range of solvent polarity. Figure 3A shows that the low energy long-wavelength (low energy) emission of **4** shows pronounced positive solvatochromism, the emissions of the other compounds, including **2**, and the short-wavelength (high-energy) minor emission peak for **4**, centered at ~400 nm, do not. This is shown in Figure 3B, which also shows that the shorter wavelength feature becomes more prominent in higher polarity solvents. Interestingly, **4** exhibited two fluorescence peaks in several polar solvents (acetonitrile, DMF, DMSO, Ethanol, EtOAc and THF), the additional peak of **4** could be due to two excited states as discussed below.

The fluorescence lifetime of carbazole itself in THF is reported as 13.7 ns by Johnson.[48] The existence of two excited states in the TCz' derivative **4** is supported by results of fluorescence-lifetime measurements, where a double-exponential decay was observed in THF

with fluorescence lifetimes of 14 and 29 ns, respectively, Table S4. However, a single-exponential adequately models the decay of **4** in some solvents towards the extremes of polarity, such as 1,4-dioxane. The average fluorescence lifetime of **4** was also found to be the highest in the series (Tables 1 and 2) while that of **2** was somewhat larger than those of **1**, **3**, **5** and **6**. The lifetimes measured for **4** were found to be independent of the emission wavelength, i.e. the same for both high- and low-energy peaks, at least in ethanol and chloroform. Fluorescence quantum yields for compounds **1**-**6** are low to medium and do not follow any obvious trend. Compounds **1**, **2**, **3**, **5** and **6** showed significantly smaller fluorescence lifetimes and emission quantum yields in chloroform than in THF, which may be indicative of quenching by charge transfer to the solvent, as observed for simple carbazole derivatives in polychlorinated solvents.[48]

A. **B.**

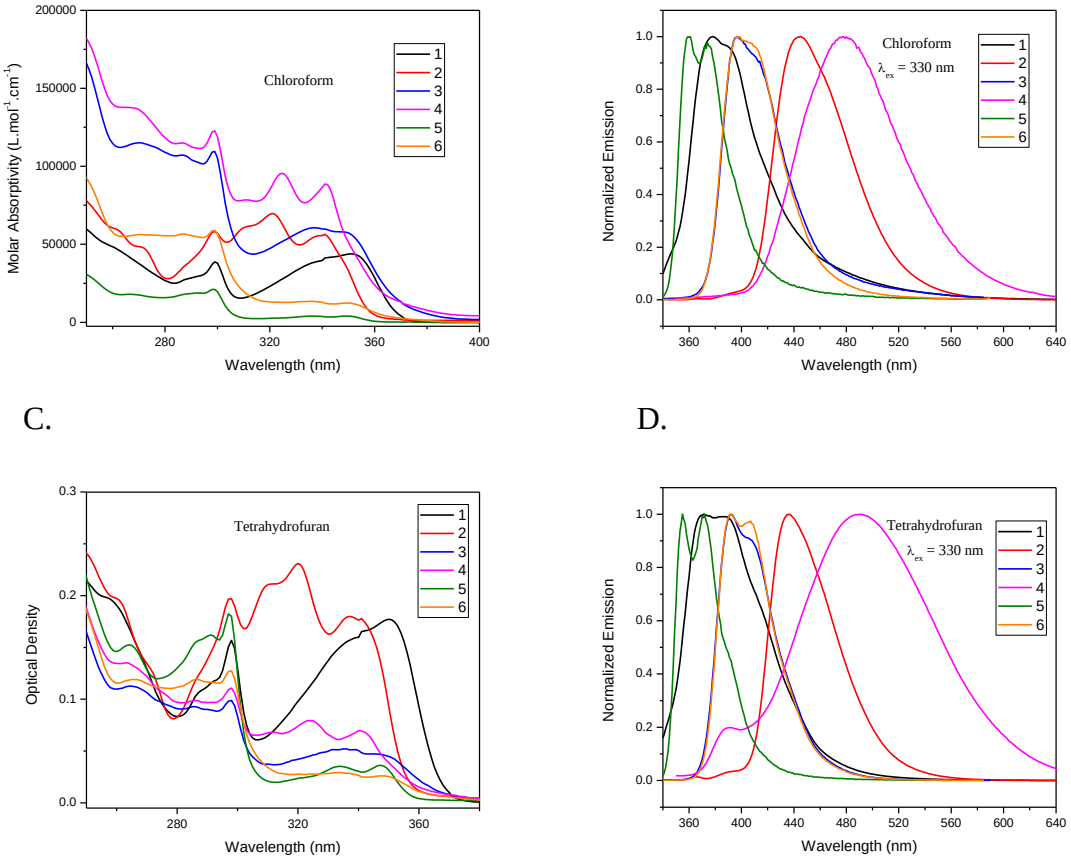

Figure 2. Absorption (A, C) and normalized emission (B, D) spectra of compounds **1 – 6** in chloroform (above) and THF (below).

Table 1. Photophysical properties of **1-6** in chloroform.

Chloroform								
#	λ_{max}^{em} / nm	λ_{max}^{abs} / nm	$\Delta\bar{\nu}$ / 10^3 cm^{-1}	τ_F / ns	τ_n / ns	Φ_F	k_r / 10^7 s^{-1}	k_{nr} / 10^7 s^{-1}
1	378	351	2.04	1.50	24	0.06	4.14	64.8
2	443	341	6.75	1.60	31	0.05	3.21	60.9
3	397	349	3.46	1.20	18	0.07	5.70	75.6
4	478	341	8.41	28.00	219	0.13	0.46	3.06
5	372	349	1.77	0.49	12	0.04	8.16	196
6	399	349	3.59	1.20	20.	0.06	5.00	78.3

λ_{max}^{em}=longest wavelength of emission; λ_{max}^{abs} longest wavelength of absorption; $\Delta\bar{\nu}$=Stokes shift; τ_F=fluorescence lifetime; τ_n=natural fluorescence lifetime; Φ_F=fluorescence quantum yield; k_r=radiative rate constant; k_{nr}=non-radiative rate constant.

Table 2. Photophysical properties of **1-6** in THF.

THF								
#	λ_{max}^{em} / nm	λ_{max}^{abs} / nm	$\Delta\bar{\nu}$ / 10^3 cm^{-1}	τ_F / ns	τ_n / ns	Φ_F	k_r / 10^7 s^{-1}	k_{nr} / 10^7 s^{-1}
1	372	350	1.69	6.2	14	0.43	7.00	9.3
2	436	344	6.13	18.0	45	0.40	2.20	3.3
3	392	347	3.31	4.7	20.	0.23	4.90	12.0
4	490	340	9.00	28.0	220	0.13	0.46	3.1
5	372	347	1.94	10.0	19	0.52	5.20	4.8
6	392	348	3.23	6.2	15	0.41	6.60	9.6

λ_{max}^{em}=longest wavelength of emission; λ_{max}^{abs} longest wavelength of absorption; $\Delta\bar{\nu}$=Stokes shift; τ_F=fluorescence lifetime; τ_n=natural fluorescence lifetime; Φ_F=fluorescence quantum yield; k_r=radiative rate constant; k_{nr}=non-radiative rate constant.

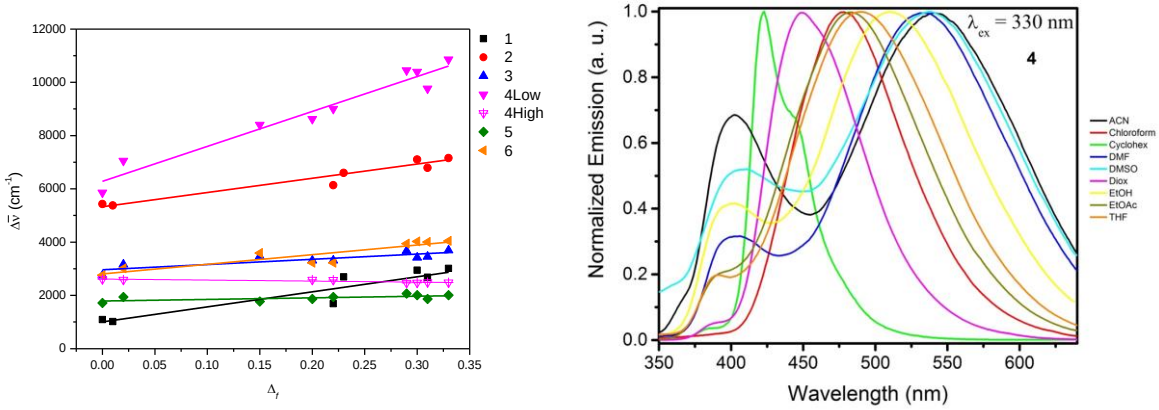

Figure 3. (A) Stokes shifts vs. orientation polarizability for compounds **1-6** (showing the low- and high-energy emission bands for **4**) in nine different solvents. (B) Normalized emission spectra of compound **4** in the nine solvents.

Electrochemical properties

The electrochemistry of new compounds **3**, **4**, and **6** were compared to those of **1**, **2**, and **5** in 0.1 M $^{n}Bu_4NPF_6$ / dichloromethane under nitrogen using cyclic voltammetry and differential pulse voltammetry (Figure 4). First we review the previously reported data for the Cz' derivatives.[41, 45] The bis-Cz' derivatives undergo two successive reversible one-electron oxidations, the separation between which originates from electronic coupling, inductive effects, and/or electrostatic interactions, between the two Cz' moieties. The somewhat larger separation, and the more facile first oxidation, seen for the THP-bridged derivative **1** is consistent with the more delocalized structure implied by the near-IR spectra of $\mathbf{1}^{\bullet+}$ vs. $\mathbf{2}^{\bullet+}$ and with a larger HOMO/HOMO–1 separation seen in DFT calculations.[45]

The TCz' model monomeric compound, **6**, undergoes three successive oxidations, consistent with the presence of three carbazole units that interact with one another, electrostatically, inductively, and/or via electronic coupling. The first oxidation occurs at a potential that is over 0.1 V less oxidizing than that of **5**. Accordingly, the bis-TCz' compounds, **3** and **4**, are expected to exhibit six oxidations, the separations between these depending on the interplay of inter- and intra-TCz' carbazole-carbazole interactions. Compound **3** exhibits four successive oxidation processes with a current ratio of 2:2:1:1; i.e., oxidations to mono- and dication occur at experimentally indistinguishable potential, as do those to $\mathbf{3}^{3+}$ and $\mathbf{3}^{4+}$, whereas oxidation to the penta- and hexacations are somewhat separated in potential. On the other hand **4** shows three oxidation processes with current ratio 1:1:1, the first two of which are seen at similar potential to those of **3**, and the third of which is seen in the same range as the third and fourth features for **3**; accordingly, we assign each of these processes to two overlapping one-electron oxidations. We note that the extent of delocalization in the mixed-valence radical cations may affect the redox potentials; optimally tuned range-separated hybrid (RSH) functional have been suggested to be reasonable approaches to describing the character of such systems with multiple oxidation (or reduction) sites,[49] and so adiabatic ionization energies (IE(g), Table 3) were determined at the OT-ωB97X-D/6-31g(d,p) level of theory. The DFT IEs fall within a narrow range of energies, and the trends in these values are mostly in qualitative agreement with the trends observed in the experimental $E^{+/0}$ redox potentials.

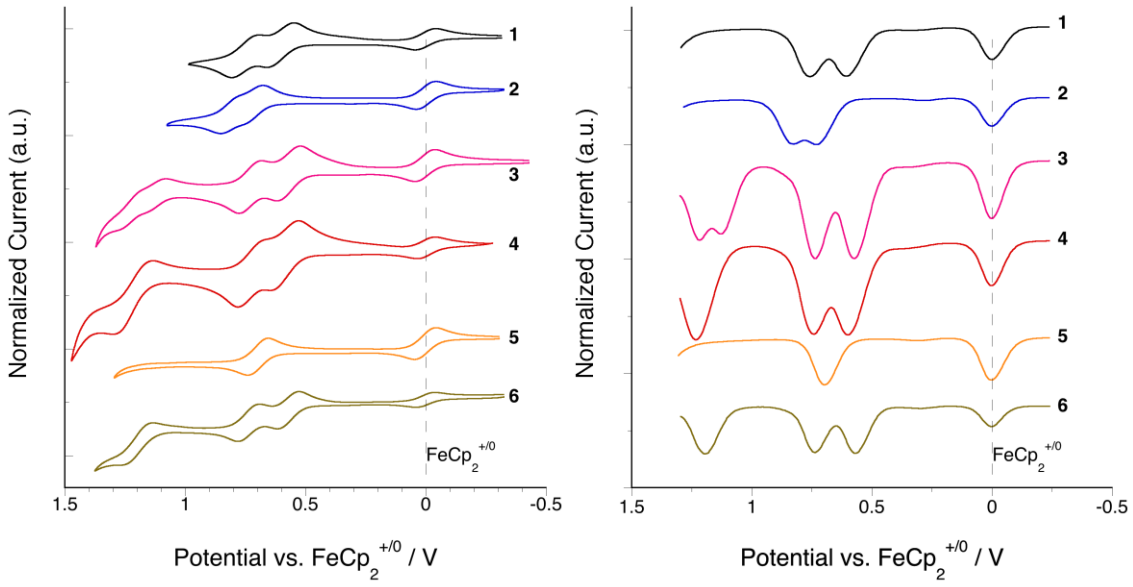

Figure 4. Cyclic voltammograms (50 mVs^{-1}) and oxidative differential pulse voltammograms of **1**-**6** in CH_2Cl_2/0.1 M nBu_4NPF_6. In each case the feature at 0 V is attributable to ferrocene, which was used as the internal standard.

Table 3. Oxidation potentials of **1**-**6** as determined in 0.1 M $^{n}Bu_4NPF_6$ in CH_2Cl_2, DFT ionization energy, and estimated solid-state energy levels.

Compound	Potentials[a] / V vs. $FeCp_2^{+/0}$						IE(g), DFT / eV[b]	Estimated energy levels / eV		
	+/0	2+/+	3+/2+	4+/3+	5+/4+	6+/5+		E_{op}[c]	IE(s)[d]	EA(s)[e]
1[41]	+0.60	+0.76	–	–	–	–	6.4	3.3	5.4	2.1
2[41]	+0.73	+0.83	–	–	–	–	6.7	3.5	5.5	2.1
3	+0.58		+0.74		+1.13	+1.22	6.4	3.4	5.4	2.0
4	+0.60		+0.74		+1.23		6.5	3.4	5.4	2.0
5[45]	+0.70	–	–	–	–	–	6.8	3.4	5.5	2.1
6	+0.57	+0.74	+1.20	–	–	–	6.7	3.4	5.4	2.0

[a]Peak potentials obtained from DPV measurements. [b]Gas-phase adiabatic IEs from OT-ωB97X-D/6-31g(d,p) calculations (OT=omega tuned). [c]Onset of optical absorption in THF. [d]Solid-state IE estimated according to $IE(s) = eE_{ox}+4.8$ eV. [e]Solid-state IE estimated according to $EA(s) = IE(s) – E_{op}$.

Organic light-emitting devices

The electroluminescence (EL) properties were characterized by using compounds **3** and **4** as active layer materials in a standard organic light-emitting device (OLED) geometry: ITO / PEDOT:PSS / **3** or **4** / Ca / Al. To facilitate hole injection and provide efficient electron-blocking,[50, 51] an additional layer of TFB (poly(9,9-dioctylfluorene-*alt*-*N*-(4-*sec*-butylphenyl)-diphenylamine)) was inserted between the PEDOT:PSS and the active material layer. The devices gave blue and bluish-green EL, with maxima in the range of 429–502 nm. Emission occurs primarily from the carbazole-material layer, with no spectral contribution from the TFB interlayer visible, although the emission of the TFB / **4** device differs from that of corresponding device without TFB (see below).

Figure 5 depicts the current density/voltage/luminance (J/V/L) characteristics of the single-layer and multi-layer devices incorporating compound **3** as the light-emitting layer. Using PEDOT and compound **3**, after a turn-on at 4.6 V, a maximum luminance of 218 cd/m^2 and a maximum current efficiency of 0.08 cd/A is reached; while using PEDOT/TFB and compound **3**, after a turn-on 5.2 V, a maximum luminance of 849 cd/m^2 and a maximum current efficacy 0.22 cd/A is achieved. The high turn-on indicates either imbalanced charge injection or transport within the devices; this is consistent with the estimated solid-state IE and EA (Table 3), low values for the latter (which, in any case, due to neglect of exciton binding energy, likely represent overestimates) suggesting that the electron-injection efficiency might be poor. The EL spectra show broad peaks with maxima at 428 and 484 nm and sky-blue CIE1931 coordinates of x = 0.18 and y = 0.21 (PEDOT/**3**) and x = 0.24 and y = 0.26 (PEDOT/TFB/**3**).

When incorporating compound **4** as emitter material, an overall superior device performance was achieved. Figure 5 depicts the corresponding current density/voltage/luminance (J/V/L) characteristics of the devices incorporating compound **4**. When using only PEDOT as the hole-transporting layer, a maximum luminance of 713 cd/m^2 was reached, with a turn-on voltage (L > 1 cd/m^2) at 3.6 V. The maximum current efficacy was 0.23 cd/A at 4.5 V. The electroluminescence spectrum (inset) for the PEDOT-based device show a broad peak with two maxima at 456 nm and 482 nm, corresponding to CIE1931 coordinates x = 0.17 and y = 0.28 (sky blue). For the devices using PEDOT/TFB and compound **4**, a maximum luminance of

1520 cd/m^2 was reached, while sacrificing turn-on voltage (V_{on} = 4.7 V). Nevertheless, maximum current efficacy rose to 0.38 cd/A at 7 V. The spectrum shows a featureless emission with a maximum that is slightly red-shifted compared to the emission spectrum of the PEDOT-only device, perhaps due to exciplex formation with the TFB. Overall, the spectrum corresponds to bluish-green CIE1931 coordinates of x = 0.23 and y = 0.44.

The turn-on voltages of 3.6 V (PEDOT/**4**) and 4.7 V (PEDOT/TFB/**4**) are generally smaller than when tetrahydropyrene-bridged molecules (4.6 V for PEDOT/**3** and 5.2 V for PEDOT/TFB/**3**) were used as the active layer. Given the fact that the energy levels of both compounds are estimated to be very similar, it is difficult to decisively conclude if this observation is due to improved electron or hole injection into the pyrene core. Note that we found a similar trend to the one observed for **1** and **2,** in devices incorporating an electron-injection layer.[41] The overall device efficiencies, however, are higher for the compounds presented herein, even in a simple single-layer device geometry. This indicates promising for these pyrene-bridged compounds as emitting materials in OLEDs. Given the fairly low estimated EAs for the present compounds, it is likely further improvement in device performance could be achieved using an additional electron-injection/transport layer (as used in our previous study of **1** and **2**).

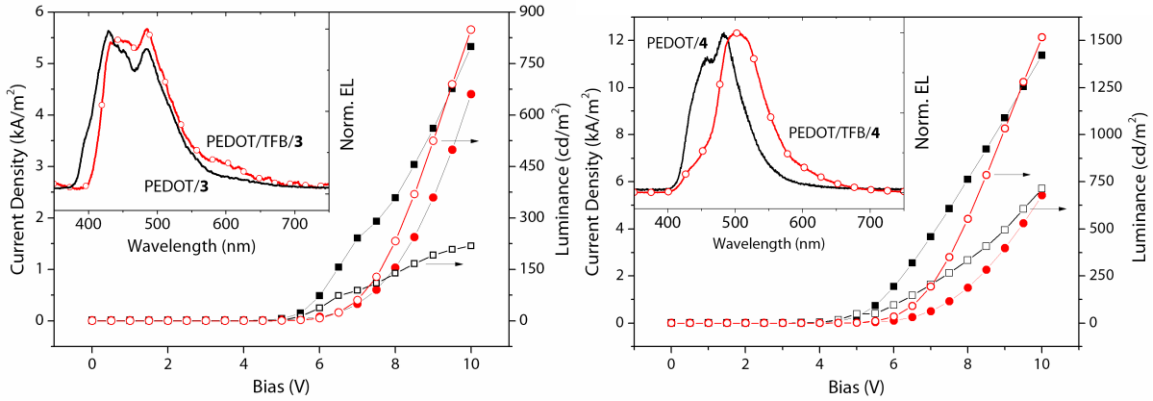

Figure 5. Current density / voltage and luminance voltage curves for OLEDs with **3** (left) and **4** (right) emissive layers with EL spectra shown as insets. By incorporating a TFB interlayer (red circles) the device efficiency improves as a result of increased luminance (open symbols) at similar current densities (filled symbols) versus the PEDOT-only devices (black squares).

Experimental Methods

General

The following compounds were synthesized according to literature procedures: 2,7-dibromo-4,5,9,10-tetrahydropyrene, **7**,[52] 2,7-dibromopyrene, **8**,[53] 3,6-di-*tert*-butyl-9*H*-carbazole, **10**,[54] and 3,6-bis(3,6-di-*tert*-butylcarbazol-*N*-yl)carbazole, **11**.[46] We previously reported the synthesis of **1**,[41] **2**,[41] and **5**.[45]

Synthesis

2,7-Bis(3,3",6,6"-tetra(*tert*-butyl)-9'*H*-9,3':6',9''-tercarbazol-9-yl)-4,5,9,10-tetrahydropyrene (3)

A 10 mL microwave tube was charged with 3,3",6,6"-tetra(*tert*-butyl)-9'*H*-9,3':6',9"-tercarbazole, **11** (625 mg, 0.866 mmol), 2,7-dibromo-4,5,9,10-tetrahydropyrene **7** (150 mg, 0.412 mmol), and a magnetic stir bar. In a glove box under nitrogen atmosphere, tris(dibenzylideneacetone)dipalladium(0) (30 mg, 0.033 mmol), tri-*tert*-butylphosphine (84 mg, 0.290 mmol), sodium *tert*-butoxide (177 mg, 1.84 mmol), and dry toluene (6 mL) were added. The tube was sealed under nitrogen and the reaction was conducted in the microwave under standard control conditions (power: 180 W; maximum temp: 150 °C; run time: 60 min; pressure: 120 psi). The reaction mixture was then poured into ice-water (100 mL) and extracted with chloroform (3 × 50 mL); the extracts were successively washed with water and brine. The solution was dried over anhydrous $MgSO_4$ and was run through a short bed of silica. The solvent was removed under reduced pressure and the resulting solid was dissolved in hot toluene and precipitated using ethanol. The obtained solid was then purified by column chromatography using hexane:dichloromethane (4:1). The solvent was removed under reduced pressure to yield **3** as beige solid (370 mg, 55%). ^{1}H NMR (500 MHz, $CDCl_3$): δ 8.18 (d, J = 2.0 Hz, 4H), 8.10 (d, J = 2.0 Hz, 8H), 7.68 (d, J = 9.0 Hz, 4H), 7.58 (dd, J = 9.0, 2.0 Hz, 4H), 7.42 (s, 4H), 7.40 (dd, J = 9.0, 2.0 Hz, 8H), 7.29 (d, J = 9.0 Hz, 8H), 3.08 (s, 8H), 1.39 (s, 72H). ^{13}C{^{1}H} NMR (125 MHz, $CDCl_3$): δ 142.53, 140.46, 140.13, 137.51, 136.16, 130.79, 129.96, 125.94, 124.70, 123.93, 123.55, 123.09, 119.30, 116.22, 111.37, 109.09, 34.73, 32.04, 28.35. HRMS-EI (*m/z*): $[M]^+$: calcd for $C_{120}H_{120}N_6$, 1644.9574; found, 1644.9625. Anal calcd for $C_{120}H_{120}N_6$: C, 87.55; H, 7.35; N, 5.10. Found: C, 87.33; H, 7.34; N, 4.92%.

2,7-Bis(3,3",6,6"-tetra(*tert*-butyl)-9'*H*-9,3':6',9"-tercarbazol-9-yl)pyrene (4)

A 10 mL microwave tube was charged with 3,3",6,6"-tetra(*tert*-butyl)-9'*H*-9,3':6',9"-tercarbazole, **11** (632 mg, 0.875 mmol), 2,7-dibromopyrene **8** (150 mg, 0.417 mmol), and a magnetic stir bar. In a glove box under nitrogen atmosphere, tris(dibenzylideneacetone)dipalladium(0) (30 mg, 0.033 mmol), tri-*tert*-butylphosphine (84 mg, 0.290 mmol), sodium *tert*-butoxide (177 mg, 1.84 mmol), and dry toluene (6 mL) were added. The tube was sealed under nitrogen and the reaction was conducted in the microwave under standard control conditions (power: 180 W; maximum temp: 150 °C; run time: 60 min; pressure: 120 psi). The reaction mixture was then poured into ice-water (100 mL) and extracted with chloroform (3 × 50 mL); the extracts were successively washed with water and brine. The solution was dried over anhydrous $MgSO_4$ and was run through a short bed of silica. The solvent was removed under reduced pressure and the resulting solid was dissolved in hot toluene and precipitated using ethanol to yield **4** as beige solid (647 mg, 95%). ^{1}H NMR (500 MHz, $CDCl_3$): δ 8.49 (s, 4H), 8.20 (d, J = 2.0 Hz, 4H), 8.15 (s, 4H), 8.11 (d, J = 2.0 Hz, 8H), 7.68 (d, J = 8.5 Hz, 4H), 7.58 (dd, J = 8.5, 2.0 Hz, 4H), 7.41 (dd, J = 8.5, 2.0 Hz, 8H), 7.32 (d, J = 8.5 Hz, 8H), 1.39 (s, 72H). ^{13}C{^{1}H} NMR (125 MHz, $CDCl_3$): δ 142.60, 140.91, 140.11, 135.34, 132.81, 131.15, 128.37, 126.14, 124.14, 123.82, 123.69, 123.59, 123.13, 119.42, 116.26, 111.01, 109.08, 34.73, 32.04. HRMS-EI (*m/z*): $[M]^+$: calcd for $C_{120}H_{116}N_6$, 1640.9261; found, 1640.9322. Anal calcd for $C_{120}H_{116}N_6$: C, 87.76; H, 7.12; N, 5.12. Found: C, 87.78; H, 6.97; N, 5.05%.

3,3'',6,6''-Tetra(*tert*-butyl)9'-(4-(*tert*-butyl)phenyl)-9'H-9,3':6',9''-tercarbazole (6)

A 10 mL microwave tube was charged with 3,3",6,6"-tetra(*tert*-butyl)-9'*H*-9,3':6',9"-tercarbazole, **11** (559 mg, 0.774 mmol), 1-bromo-4-*tert*-butylbenzene **9** (150 mg, 0.704 mmol), and a magnetic stir bar. The tube was sealed and was degassed with nitrogen for 10 min. In a glove box under nitrogen atmosphere, tris(dibenzylideneacetone)dipalladium(0) (26 mg, 0.028 mmol), tri-*tert*-butylphosphine (84 mg, 0.241 mmol), sodium *tert*-butoxide (150 mg, 1.56 mmol), and dry toluene (6 mL) were added. The tube was sealed under nitrogen and the reaction was conducted in the microwave under standard control conditions (power: 180 W; maximum temp: 150 °C; run time: 60 min; pressure: 120 psi). The reaction mixture was then poured into ice-water (100 mL)

and extracted with chloroform (3 × 50 mL); the extracts were successively washed with water and brine. The solution was dried over anhydrous $MgSO_4$ and was run through a short bed of silica. The obtained solid was then purified by column chromatography using hexane:DCM (7:1). The solvent was removed under reduced pressure to yield **6** as beige solid (383 mg, 64%). ^{1}H NMR (500 MHz, $CDCl_3$): δ 8.15 (d, J = 1.5 Hz, 2H), 8.09 (d, J = 2.0 Hz, 4H), 7.63 (d, J = 8.5 Hz, 2H), 7.58-7.56 (m, 4H), 7.52 (dd, J = 8.5, 1.5 Hz, 2H), 7.39 (dd, J = 8.5, 2.0 Hz, 4H), 7.27 (d, J = 8.5 Hz, 4H), 1.39 (s, 45H). ^{13}C{^{1}H} NMR (125 MHz, $CDCl_3$): δ 151.15, 142.46, 140.53, 140.13, 134.43, 130.60, 127.05, 126.64, 125.84, 123.77, 123.52, 123.03, 119.21, 116.17, 111.24, 109.07, 34.89, 34.71, 32.03, 31.43. HRMS-EI (*m/z*): $[M]^+$: calcd for $C_{62}H_{67}N_3$, 853.5335; found, 853.5155. Anal calcd for $C_{62}H_{67}N_3$: C, 87.17; H, 7.91; N, 4.92. Found: C, 86.89; H, 7.75; N, 4.80%.

Photophysical Studies

Absorption spectra were measured using a double-beam JASCO V-570. UV-vis-NIR spectrophotometer, and the fluorescence measurements were performed using a Jobin-Yvon-Horiba Fluorolog III spectrofluorometer. The excitation source was a 100 W xenon lamp, and the detector used was R-928 operating at a voltage of 950 V. Right-angle mode detection was used. Slit widths were fixed at 5 nm for both entrance and exit slits during both emission and excitation experiments. Corrected emission spectra S_1/R_1 were collected to account for any fluctuation in the xenon lamp over different wavelengths. In parallel to that, S_1 spectra were collected to make sure that the intensity of emission is below 2×10^6 counts per second in order to avoid saturation of the detector. A blank measurement with no sample in the sample holder was subtracted from all actual spectra to account for any error possible due to the sample holder. Stock solutions of concentration ranging from 0.5-5 mM of each compound were prepared in chloroform depending on the solubility limit of each compound. Around 0.1 mL of each stock solution was transferred into nine dry glass vials and chloroform was left to evaporate. Then the corresponding solvent was added and diluted to 100 µM for absorption measurements and to 1-2 µM for fluorescence studies. Stock solutions were kept in the freezer and discarded if not used within two days. Molar absorptivity was determined in chloroform. Quantum yields were measured using 9,10-diphenylanthracene in cyclohexane as standard with an attributed quantum yield of 1.00. The excitation wavelength was set to 330 nm for all compounds and the standard.

Quantum yield measurements were performed on nitrogen-purged solutions, and optical density was maintained below 0.05 for all samples. UV-transparent quartz cuvette (1 × 1 cm) was used for all experiments. Molar absorptivity and quantum yield were performed as three runs for each compound in every single solvent, and the average value of the three runs was reported. A fourth run was performed in cases where inconsistent results were obtained in one of the first three runs.

Electrochemistry

Cyclic voltammetry and differential pulse voltammetry was carried out in solutions of tetra-n-butylammounim hexafluorophosphate (0.1 M) in dry dichloromethane using a glassy carbon woking electrode, a platinum wire counter electrode, a Ag wire anodized in 1 M aqueous KCl as a pseudo reference electrode, and a CH Instruments potentiostat. Ferrocene ($FeCp_2$) was used as an internal standard. Cyclic voltammetry was carried out with a scan rate of 0.05 V/s, while differential pulse voltammetry with a scan amplitude of 0.05 V, pulse width 0.2 s, sampling width 0.0167 s, and a pulse period of 0.5 s.

Organic light-emitting device fabrication and characterization

Devices were fabricated on pre-patterned ITO substrates (Psiotec Ltd), which were mechanically cleaned with acetone and sonicated in isopropanol, followed by oxygen plasma treatment (Diener Femto). A 45 nm thick PEDOT:PSS film (Clevios AI4083) was spin coated on top and annealed for 10 min at 220 °C in air. TFB (American Dye Source) was deposited by spin coating from a 6 mg/ml solution in toluene and dried under vacuum for 1 h at 200 °C to yield a < 10 nm film. The emissive layers were spin coated from 6 mg/ml solution in toluene to yield 30 nm thick films. Ca (5 nm) and Al (200 nm) electrodes were deposited through a shadow mask at a base pressure of 10^{-6} mbar in a thermal evaporator to form multiple devices with an active area of 4 mm^2. The devices were encapsulated using a UV-curable epoxy (Ossila Ltd.) and a glass cover slide. Morphological analysis of device layers were carried out according to previously reported methodology.[51] Current density/voltage/luminance characteristics were recorded using a Keithley 2450 source measurement unit, together with a Konica Minolta LS-160 luminance meter in a custom setup. Electroluminescence spectra were acquired using an Ocean Optics HR2000+ spectrometer.

Density Functional Theory (DFT) Calculations

The density functional theory (DFT) and time-dependent DFT (TDDFT) calculations were carried out at the OT-ωB97X-D/6-31g(d,p) (OT = optimally tuned) level of theory.[55-57] For each molecule considered, the ω parameter was iteratively tuned via the gap-tuning[58-61] procedure, and the tuned ω used for each subsequent DFT and TDDFT calculation. All optimized, unconstrained geometries were confirmed as minima through normal mode analyses. To reduce the computational costs, all *tert*-butyl groups were truncated to methyl groups. The Gaussian09 (Revision E.01)c[62] software suite was used for all DFT and TDDFT calculations.

Conclusions

The new bis-TCz' compounds **3** and **4** can be synthesized in a similar way to their Cz' analogues **1** and **2**. Their photophysical properties have been studied in a variety of solvents; interestingly **4** exhibits clear dual emission, with the longer-wavelength emission being more markedly Stokes-shifted than that of the other compounds and also more solvatochromic and exhibiting a considerably longer lifetime. Electrochemical studies indicate up to six electrons can be reversible removed from both **3** and **4**. Both compounds have been tested in simple OLEDs that are more efficient than devices we have previously reported based on use of **1** and **2** in slightly more complex architectures; however, the electroluminescence of the **3**- and **4**-based devices is sky blue to green-blue, whereas those using **1** and **2** emit in the deep blue.

Acknowledgments

This work was supported by the University Research Board (URB) of the American University of Beirut, the Lebanese National Council for Scientific Research (CNRS), and the Kamal A. Shair CRSL. The authors are grateful for this support. B. R. K. and B.W. thank the Arab Fund Scholarship Program for financial support. S. R. M. thanks the Alexander Humboldt Foundation for support. The work at the University of Kentucky was supported by the Department of the Navy, Office of Naval Research, ONR Award No. N00014-16-1-2985. Supercomputing resources on the Lipscomb High Performance Computing Cluster were provided by the

University of Kentucky Information Technology Department and Center for Computational Sciences (CCS).

Electronic Supporting Information

Photophysical data in different solvents, Stokes shifts, frontier molecular orbitals, NTO analysis, NMR spectra, and film studies.

References

1. X. L. Hao, L. Zhang, D. Wang, C. Zhang, J. F. Guo and A. M. Ren, *J. Phys. Chem. C*, 2018, **122**, 6273-6287.
2. J. F. Xing, W. Q. Chen, J. Gu, X. Z. Dong, N. Takeyasu, T. Tanaka, X. M. Duan and S. Kawata, *J. Mater. Chem.*, 2007, **17**, 1433-1438.
3. C. Huang, M. M. Sartin, N. Siegel, M. Cozzuol, Y. D. Zhang, J. M. Hales, S. Barlow, J. W. Perry and S. R. Marder, *J. Mater. Chem.*, 2011, **21**, 16119-16128.
4. X. H. Ouyang, H. P. Zeng and W. Ji, *J. Phys. Chem. B*, 2009, **113**, 14565-14573.
5. B. Kippelen, S. R. Marder, E. Hendrickx, J. L. Maldonado, G. Guillemet, B. L. Volodin, D. D. Steele, Y. Enami, Sandalphon, Y. J. Yao, J. F. Wang, H. Rockel, L. Erskine and N. Peyghambarian, *Science*, 1998, **279**, 54-57.
6. J. Lu, P. F. Xia, P. K. Lo, Y. Tao and M. S. Wong, *Chem. Mater.*, 2006, **18**, 6194-6203.
7. R. S. Kularatne, H. D. Magurudeniya, P. Sista, M. C. Biewer and M. C. Stefan, *J. Polym. Sci. Pol. Chem.*, 2013, **51**, 743-768.
8. S. Beaupre and M. Leclerc, *J. Mater. Chem. A*, 2013, **1**, 11097-11105.
9. O. Kwon, S. Barlow, S. A. Odom, L. Beverina, N. J. Thompson, E. Zojer, J.-L. Brédas and S. R. Marder, *J. Phys. Chem. A*, 2005, **109**, 9346-9352.
10. F. Dumur, *Org. Electron.*, 2015, **25**, 345-361.
11. C. W. Tang and S. A. VanSlyke, *Appl. Phys. Lett.*, 1987, **51**, 913-915.
12. C. Adachi, *Jpn. J. Appl. Phys.*, 2014, **53**, 060101.
13. M. A. Baldo, D. F. O'Brien, Y. You, A. Shoustikov, S. Sibley, M. E. Thompson and S. R. Forrest, *Nature*, 1998, **395**, 151-154.
14. M. Segal, M. A. Baldo, R. J. Holmes, S. R. Forrest and Z. G. Soos, *Phys. Rev. B*, 2003, **68**.
15. T. Miwa, S. Kubo, K. Shizu, T. Komino, C. Adachi and H. Kaji, *Sci. Rep.*, 2017, **7**, 284.
16. H. Uoyama, K. Goushi, K. Shizu, H. Nomura and C. Adachi, *Nature*, 2012, **492**, 234-238.
17. Z. Yang, Z. Mao, Z. Xie, Y. Zhang, S. Liu, J. Zhao, J. Xu, Z. Chi and M. P. Aldred, *Chem. Soc. Rev.*, 2017, **46**, 915-1016.
18. B. Wex and B. R. Kaafarani, *J. Mater. Chem. C*, 2017, **5**, 8622-8653.
19. M. Y. Wong and E. Zysman-Colman, *Adv. Mater.*, 2017, **29**, 1605444.
20. Y. Im, M. Kim, Y. J. Cho, J.-A. Seo, K. S. Yook and J. Y. Lee, *Chem. Mater.*, 2017, **29**, 1946-1963.
21. C.-Y. Chan, L.-S. Cui, J. U. Kim, H. Nakanotani and C. Adachi, *Adv. Funct. Mater.*, 2018, **28**, 1706023.
22. D. Tavgeniene, L. Liu, G. Krucaite, D. Volyniuk, J. V. Grazulevicius, Z. Xie, B. Zhang and S. Grigalevicius, *J. Electron. Mater.*, 2015, **44**, 4006-4011.

23. J.-F. Morin, M. Leclerc, D. Adès and A. Siove, *Macromol. Rapid Commun.*, 2005, **26**, 761-778.
24. M. Ates and N. Uludag, *J. Solid State Electr.*, 2016, **20**, 2599-2612.
25. O. Usluer, S. Demic, D. A. M. Egbe, E. Birckner, C. Tozlu, A. Pivrikas, A. M. Ramil and N. S. Sariciftci, *Adv. Funct. Mater.*, 2010, **20**, 4152-4161.
26. Z.-a. Li, Z. Jiang, S. Ye, C. K. W. Jim, G. Yu, Y. Liu, J. Qin, B. Z. Tang and Z. Li, *J. Mater. Chem.*, 2011, **21**, 14663-14671.
27. W. Li, J. Li, D. Liu and Q. Jin, *ACS Appl. Mater. Inter.*, 2016, **8**, 22382-22391.
28. T. Nishimoto, T. Yasuda, S. Y. Lee, R. Kondo and C. Adachi, *Mater. Horiz.*, 2014, **1**, 264-269.
29. W. Jiang, L. Duan, J. Qiao, G. Dong, D. Zhang, L. Wang and Y. Qiu, *J. Mater. Chem.*, 2011, **21**, 4918-4926.
30. P. L. Santos, J. S. Ward, P. Data, A. S. Batsanov, M. R. Bryce, F. B. Dias and A. P. Monkman, *J. Mater. Chem. C*, 2016, **4**, 3815-3824.
31. P. Rajamalli, N. Senthilkumar, P. Gandeepan, C.-C. Ren-Wu, H.-W. Lin and C.-H. Cheng, *ACS Appl. Mater. Inter.*, 2016, **8**, 27026-27034.
32. Q. Zhang, Y. F. Hu, Y. X. Cheng, G. P. Su, D. G. Ma, L. X. Wang, X. B. Jing and F. S. Wang, *Synth. Met.*, 2003, **137**, 1111-1112.
33. X. He, D. Cai, D.-Y. Kang, W. Haske, Y. Zhang, C. A. Zuniga, B. H. Wunsch, S. Barlow, J. Leisen, D. Bucknall, B. Kippelen and S. R. Marder, *J. Mater. Chem. C*, 2014, **2**, 6743-6751.
34. S. J. Kim, J. Leroy, C. Zuniga, Y. D. Zhang, L. Y. Zhu, J. S. Sears, S. Barlow, J.-L. Brédas, S. R. Marder and B. Kippelen, *Org. Electron.*, 2011, **12**, 1314-1318.
35. C. A. Zuniga, J. Abdallah, W. Haske, Y. D. Zhang, I. Coropceanu, S. Barlow, B. Kippelen and S. R. Marder, *Adv. Mater.*, 2013, **25**, 1739-1744.
36. J. Nishide, H. Nakanotani, Y. Hiraga and C. Adachi, *Appl. Phys. Lett.*, 2014, **104**, 233304.
37. K. Y. Sun, W. Jiang, X. X. Ban, B. Huang, Z. H. Zhang, M. Y. Ye and Y. M. Sun, *RSC Adv.*, 2016, **6**, 22137-22143.
38. S. Hirata, Y. Sakai, K. Masui, H. Tanaka, S. Y. Lee, H. Nomura, N. Nakamura, M. Yasumatsu, H. Nakanotani, Q. S. Zhang, K. Shizu, H. Miyazaki and C. Adachi, *Nat. Mater.*, 2015, **14**, 330-336.
39. N. D. McClenaghan, R. Passalacqua, F. Loiseau, S. Campagna, B. Verheyde, A. Hameurlaine and W. Dehaen, *J. Am. Chem. Soc.*, 2003, **125**, 5356-5365.
40. W. Jiang, L. A. Duan, J. A. Qiao, G. F. Dong, D. Q. Zhang, L. D. Wang and Y. Qiu, *J. Mater. Chem.*, 2011, **21**, 4918-4926.
41. B. R. Kaafarani, A. a. O. El-Ballouli, R. Trattnig, A. Fonari, S. Sax, B. Wex, C. Risko, R. S. Khnayzer, S. Barlow, D. Patra, T. V. Timofeeva, E. J. W. List, J.-L. Brédas and S. R. Marder, *J. Mater. Chem. C*, 2013, **1**, 1638-1650.
42. J. F. Ambrose, L. L. Carpenter and R. F. Nelson, *J. Electrochem. Soc.*, 1975, **122**, 876-894.
43. K. Karon and M. Lapkowski, *J. Solid State Electr.*, 2015, **19**, 2601-2610.
44. M.-H. Ho, B. Balaganesan, T.-Y. Chu, T.-M. Chen and C. H. Chen, *Thin Solid Films*, 2008, **517**, 943-947.
45. B. R. Kaafarani, C. Risko, T. H. El-Assaad, A. a. O. El-Ballouli, S. R. Marder and S. Barlow, *J. Phys. Chem. C*, 2016, **120**, 3156-3166.

46. N. Prachumrak, S. Pansay, S. Namuangruk, T. Kaewin, S. Jungsuttiwong, T. Sudyoadsuk and V. Promarak, *Eur. J. Org. Chem.*, 2013, **2013**, 6619-6628.
47. S. Sasaki, G. P. C. Drummen and G.-i. Konishi, *J. Mater. Chem. C*, 2016, **4**, 2731-2743.
48. G. E. Johnson, *J. Phys. Chem.*, 1980, **84**, 2940-2946.
49. C. Sutton, T. Körzdörfer, V. Coropceanu and J.-L. Brédas, *J. Phys. Chem. C*, 2014, **118**, 3925-3934.
50. S. A. Choulis, V.-E. Choong, A. Patwardhan, M. K. Mathai and F. So, *Adv. Funct. Mater.*, 2006, **16**, 1075-1080.
51. R. Trattnig, L. Pevzner, M. Jäger, R. Schlesinger, M. V. Nardi, G. Ligorio, C. Christodoulou, N. Koch, M. Baumgarten, K. Müllen and E. J. W. List, *Adv. Funct. Mater.*, 2013, **23**, 4897-4905.
52. D. Rausch and C. Lambert, *Org. Lett.*, 2006, **8**, 5037-5040.
53. H. Lee and R. G. Harvey, *J. Org. Chem.*, 1986, **51**, 2847-2848.
54. Y. Liu, M. Nishiura, Y. Wang and Z. Hou, *J. Am. Chem. Soc.*, 2006, **128**, 5592-5593.
55. J.-D. Chai and M. Head-Gordon, *Phys. Chem. Chem. Phys.*, 2008, **10**, 6615-6620.
56. M. M. Francl, W. J. Pietro, W. J. Hehre, J. S. Binkley, M. S. Gordon, D. J. DeFrees and J. A. Pople, *J. Chem. Phys.*, 1982, **77**, 3654-3665.
57. P. C. Hariharan and J. A. Pople, *Theoret. Chim. Acta*, 1973, **28**, 213-222.
58. T. Stein, H. Eisenberg, L. Kronik and R. Baer, *Phys. Rev. Lett.*, 2010, **105**, 266802.
59. T. Stein, L. Kronik and R. Baer, *J. Am. Chem. Soc.*, 2009, **131**, 2818-2820.
60. T. Stein, L. Kronik and R. Baer, *J. Chem. Phys.*, 2009, **131**, 244119.
61. S. Refaely-Abramson, R. Baer and L. Kronik, *Phys. Rev. B*, 2011, **84**, 075144.
62. Gaussian 09, Revision E.01, M. J. Frisch, G. W. Trucks, H. B. Schlegel, G. E. Scuseria, M. A. Robb, J. R. Cheeseman, G. Scalmani, V. Barone, B. Mennucci, G. A. Petersson, H. Nakatsuji, M. Caricato, X. Li, H. P. Hratchian, A. F. Izmaylov, J. Bloino, G. Zheng, J. L. Sonnenberg, M. Hada, M. Ehara, K. Toyota, R. Fukuda, J. Hasegawa, M. Ishida, T. Nakajima, Y. Honda, O. Kitao, H. Nakai, T. Vreven, J. A. Montgomery, Jr., J. E. Peralta, F. Ogliaro, M. Bearpark, J. J. Heyd, E. Brothers, K. N. Kudin, V. N. Staroverov, R. Kobayashi, J. Normand, K. Raghavachari, A. Rendell, J. C. Burant, S. S. Iyengar, J. Tomasi, M. Cossi, N. Rega, J. M. Millam, M. Klene, J. E. Knox, J. B. Cross, V. Bakken, C. Adamo, J. Jaramillo, R. Gomperts, R. E. Stratmann, O. Yazyev, A. J. Austin, R. Cammi, C. Pomelli, J. W. Ochterski, R. L. Martin, K. Morokuma, V. G. Zakrzewski, G. A. Voth, P. Salvador, J. J. Dannenberg, S. Dapprich, A. D. Daniels, Ö. Farkas, J. B. Foresman, J. V. Ortiz, J. Cioslowski, and D. J. Fox, Gaussian, Inc., Wallingford CT, 2009.

TOC

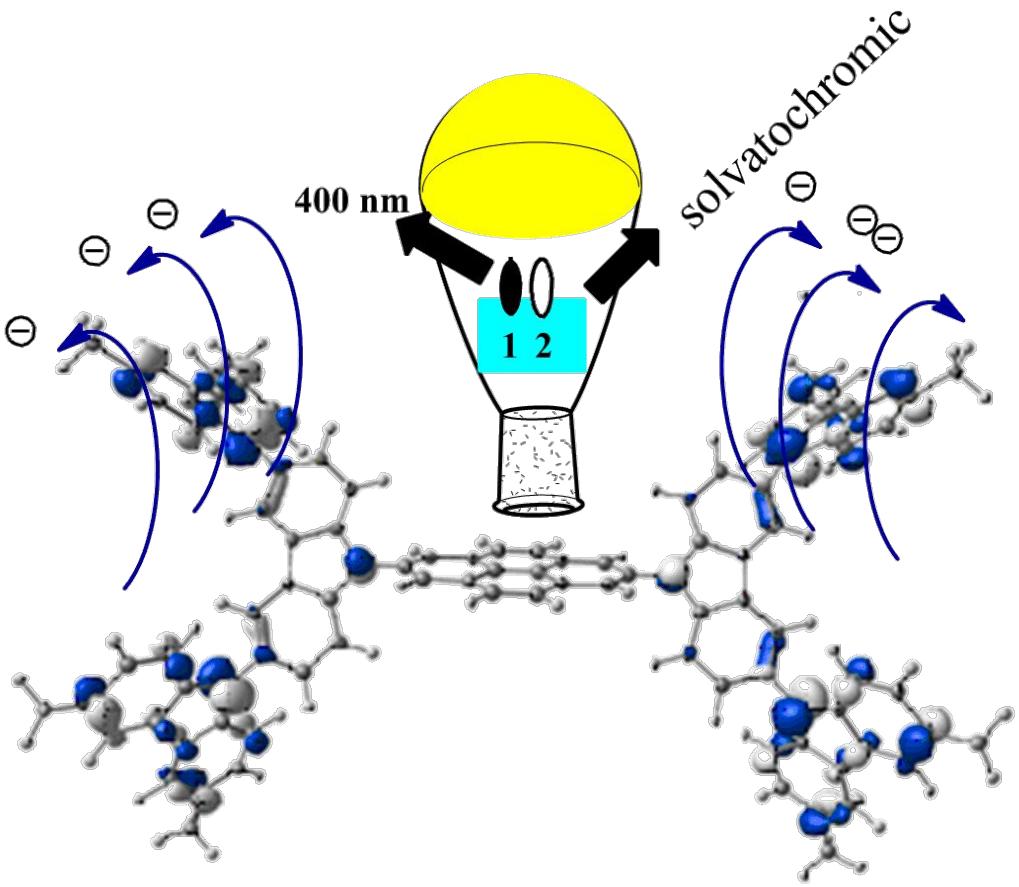

Bis(tercarbazole) derivatives of tetrahydropyrene and pyrene are compared to their bis(carbazole) analogues. The bis(tercarbazole) derivatives can be reversibly oxidized up to hexacations. One example shows solvent-dependent dual emission behavior. Blue- to blue-green-emitting OLEDs have been fabricated using the bis(tercarbazole)s as the emissive layer.